Hierarchically Fractal PtPdCu Sponges and their Directed Mass- and Electron-Transfer Effects

Yu-Xuan Xiao,[‡] Jie Ying,[†] Ge Tian,[‡] Xiong Yang,[‡] Yue-Xing Zhang,[§] Jiang-Bo Chen,[‡] Yong Wang,[‡] Mark D. Symes,[//] Kenneth I. Ozoemena,[⊥] Jinsong Wu,[‡] Xiao-Yu Yang[*‡#]*

[†]*School of Chemical Engineering and Technology, Sun Yat-sen University, Zhuhai, 519082, China.*

[‡]*State Key Laboratory of Advanced Technology for Materials Synthesis and Processing & School of Materials Science and Engineering & NRC (Nanostructure Research Centre), Wuhan University of Technology, Wuhan, 430070, China.*

[§]*College of Chemistry and Chemical Engineering, Hubei University, Wuhan, 430062, China.*

[//]*WestCHEM, School of Chemistry, University of Glasgow, University Avenue, Glasgow, G12 8QQ, UK.*

[⊥]*Molecular Sciences Institute, School of Chemistry, University of the Witwatersrand, Private Bag 3, Johannesburg 2050, South Africa.*

[#]*School of Engineering and Applied Sciences, Harvard University, Cambridge, Massachusetts 02138, USA.*

KEYWORDS: Pt-based alloy, fractal structure, hollow porous structure, directed transfer effect, methanol oxidation reaction

ABSTRACT: Fractal Pt-based materials with hierarchical structures and high self-similarity have attracted more and more attention due to their bio-inspiring maximum optimization of energy utilization and mass transfer. However, their high efficiency design of the mass- and electron-transfer still remains great challenges. Herein, fractal PtPdCu hollow sponges (denoted as PtPdCu-HS) facilitating both directed mass- and electron-transfer are presented. Such directed transfer effects greatly promote electrocatalytic activity, regarding as 3.9 times the mass activity, 7.3 times the specific activity, higher poison tolerance, and higher stability than commercial Pt/C for the methanol oxidation reaction (MOR). A new "directed mass- and electron-transfer" concept, characteristics, and mechanism are proposed at the micro/nanoscale to clarify the structural design and functional enhancement of fractal electrocatalyst. This work displays new possibilities for designing novel nanomaterials with high activity and superior stability towards electrocatalysis or other practical applications.

Platinum (Pt)-based nanostructures have been one of the most effective catalysts applied in electrocatalysis, and thus discovery of novel nanostructures has been one of the main strategies to enhance their performance.[1-4] Recent experimental and theoretical progresses on electrochemical reactions have revealed two critical factors for high-performance design. Firstly, maximum utilization of electronic energy is critical for the development of highly active facets and alloying stress structures with high intrinsic conductivity and electrochemical activity.[5-9] The other is to optimize diffusion of matter and hence increase the contact possibility between the active sites and reactants, which strongly depends on nanoscale adjustment, morphological control, surface roughness, structure porosity and/or their synergistic effects.[10-14] Undoubtedly, the development of Pt-based nanostructures with minimum energy loss and the most efficient matter transfer is highly desired, although almost all approaches in previous reports generally require for such a combination.

Fractal hierarchy is the most common structure in nature and many classes of organisms among both plants and animals contain fractal structure to maximize the mass transport and increase the rates of reactions for optimal efficiency and least energy consumption.[15-17] A unique feature of fractals is the directed transfer phenomenon, for example, both water transport and photogenerated efficient electron transfer in trees are mainly achieved from the main stems to the smaller branches in a directed way.[18] This feature dictates the outstanding transfer and utilization efficiency of energy and matter in natural substances. In materials design, fractal functions, often appearing in their hierarchical micro/nanostructures with high self-similarity, have attracted more and more attention.[19,20] Significant progress has been made to implement fractal structures, such as fractal zeolites,[21,22] graphenes,[23-25] oxides/selenides,[26-28] and metals,[29-32] in areas ranging from nanoscience to catalysis, separation, energy, life science and other applications. There have been

advances on synthetic approaches to fractal Pt-based nanostructures, including hard fractal-templating,[33-35] surfactant templating,[36-38] and electro-deposition.[39-41] However, it is not easy to achieve direct synthesis of Pt-based fractals under mild conditions, such as open system, room temperature, and aqueous solvent, which is critical for scale-up for practical applications.[33,37] Furthermore, each of these previous Pt-based fractal studies addresses mainly structural aspects, while their high electron transfer efficiency has not been thoroughly investigated for promising applications, particularly in catalysis and electrocatalysis. Thus, a directed transfer investigation of both energy and matter on Pt-based fractal design for electrocatalysis would be a significant advance.

Considering the above, we herein present a facile and efficient approach to direct synthesis of fractal PtPdCu sponges (denoted as PtPdCu-S) by galvanic replacement at room-temperature using aqueous solvent in an open system. To further optimize the pore structure by Pd-Cu co-etching, the resulting PtPdCu-HS (denoted as PtPdCu-HS) with three-dimensional (3D) hierarchically fractal pores not only provide directed transportation of reactants from large sized pores to small sized pores, but also maintain directed transfer of electrons from the thick walls of large sized pores to the thinner walls of small sized pores. Such a fractal structure shows a very high surface area and rich surface-active sites. Density functional theory (DFT) results further indicate a 23.5% increase of surface atomic number as well as a 4.3% increase in surface area in comparison with non-fractal nanostructures. Moreover, PtPdCu-HS exhibits outstanding electrocatalytic properties, including high electrocatalytic activity, unusual poison tolerance, and excellent stability in the methanol oxidation reaction (MOR). The mechanism of synthesis of these materials and the directed mass- and electron-transfer effects on the enhancement of the resulting electrocatalytic activity have also been fully explored.

The morphological and structural characterization of PtPdCu-HS is shown in Figure 1. Figure 1a clearly shows that PtPdCu-HS has multilevel generations with a long main trunk and many well-aligned side branches, resembling a fractal tree. The length of the trunk is about 7 μm, while the branches range from 0.5 μm to 3 μm. Moreover, closer observation finds that each branch also exhibits a hierarchical fractal structure, which is composed of a main branch and sub-branches (Figure 1b). The centers of these branches are brighter than the edges, clearly depicting a hollow feature. Transmission electron microscopy (TEM) images with higher magnification show that the branches are composed of numerous small nanoparticles, which are fused together to form an open interconnected porous system (Figure 1c). As shown in Figure S1a, these particles exhibit a mean size distribution of 3.7 ± 0.7 nm. Figure 1d shows the selected area electron diffraction (SAED) pattern recorded from the branches in Figure 1b. The five diffraction rings can be indexed to the (111), (200), (220), (311) and (222) facets, respectively. Figure 1e and f show the lattices fringes and the corresponding fast Fourier transform (FFT) results from one nanoparticle in Figure 1c. As can be seen, the lattice fringe of 0.221 nm is close to the 0.223 nm for Pt(111) facets, proving the nanoparticle is well enclosed by (111) facets. Figure 1g-i show the high-angle annular dark field-scanning TEM (HAADF-STEM) images of PtPdCu-HS. Under dark field, the porous and hollow features can be witnessed more clearly (Figure 1g). The thickness of pore walls was measured in Figure 1h, and the results shown that the main branch has a thicker pore wall (20.8 nm) than that in the sub-branch (11.9 nm). Moreover, the size of main pore (102 nm) is also bigger than that of the sub-pore (42.5 nm). Similar phenomena can be found in other branches (Figure S2). Figure 1i-m show the HAADF-STEM image of nanoparticles in the branches and corresponding elemental mapping results, indicating a Pt-rich alloying structure and a homogeneous dispersion of Pt, Pd and Cu in PtPdCu-HS. Moreover, inductively coupled plasma-atomic emission spectrometry (ICP-

AES) results show that the atomic ratio of Pt, Pd, and Cu in PtPdCu-HS is close to 8:1:1, further proving the Pt-rich structure of PtPdCu-HS. Compared to PtPdCu-S (see Figure S3 for detailed TEM characterization), PtPdCu-HS after acid treatment exhibits richer porous and finer alloyed structure.

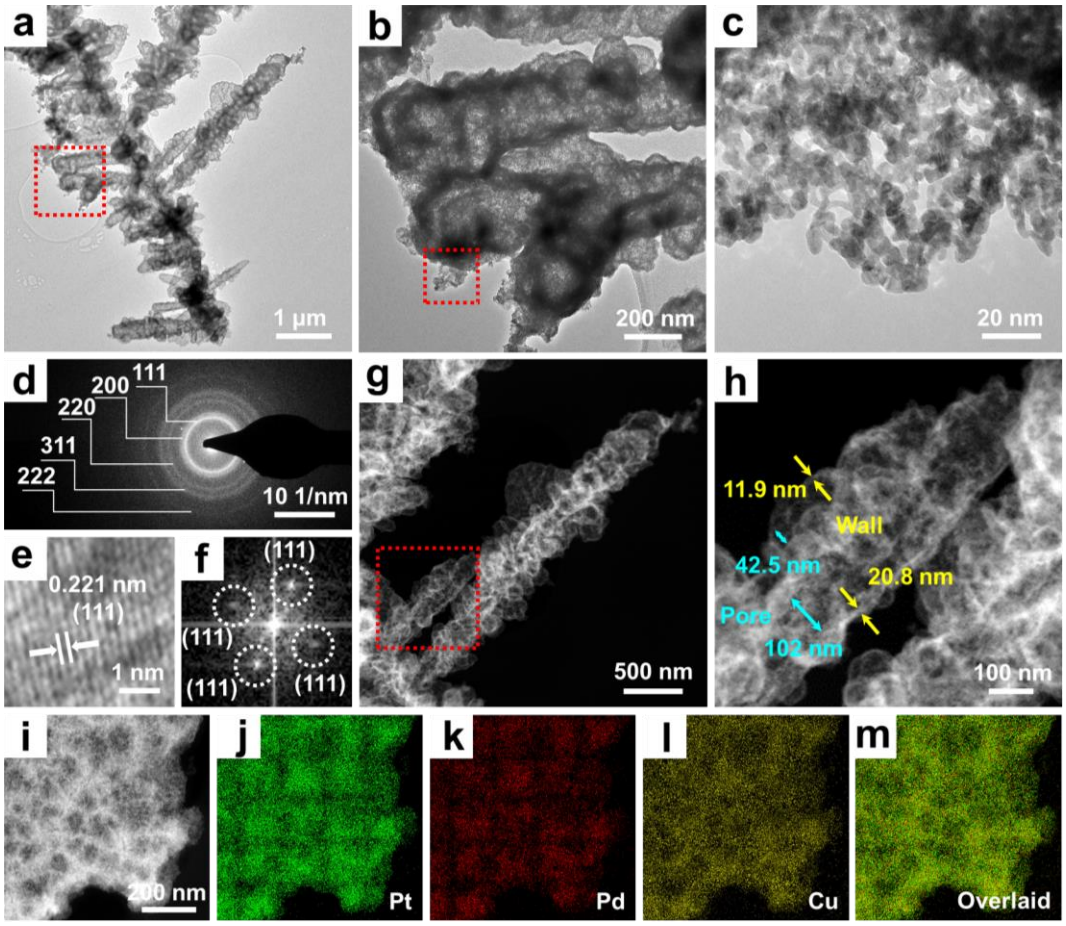

Figure 1. (a-c) TEM images of PtPdCu-HS with different magnifications. (d) Electron diffraction pattern of b. (e) Lattice fringes and (f) corresponding FFT result of c. (g-i) HAADF-STEM image of PtPdCu-HS with different magnifications. EDX elemental mapping results of (j) Pt, (k) Pd, (l) Cu, and (m) PtPdCu overlaid color mapping.

Figure 2 shows more detailed comparison of PtPdCu-S and PtPdCu-HS. As shown in Figure 2a, the four peaks of PtPdCu-S and PtPdCu-HS match well with face-centered cubic (fcc) Pt (ICDD no. 04-0802), Pd (ICDD no. 46-1043), and Cu (ICDD no. 85-1326), which are in agreement with those of the previous reports.[42,43] After HNO_3 treatment, most of the Pd and Cu were selectively removed, leaving Pt-enriched hollow structures of PtPdCu-HS, and the peaks of PtPdCu-HS show an obvious shift towards lower 2 theta values, suggesting extension of the lattice parameters due to the removal of Pd and Cu. The surface areas and porosities of PtPdCu-S and PtPdCu-HS were measured by N_2 physisorption isotherms (Figure 2b), which indicate mesoporous structures for both PtPdCu-S and PtPdCu-HS. The Brunauer-Emmett-Teller (BET) surface area of PtPdCu-S was determined to be 46 m^2 g^{-1}. After HNO_3 treatment, due to the formation of hollow structures, the BET surface area of PtPdCu-HS increases a lot and reaches remarkably 107 m^2 g^{-1}, which is rare in metal-based catalysts (Figure S4 and Table S1). Figure S5 shows the pore size distribution results of PtPdCu-HS and PtPdCu-S. As can be seen, PtPdCu-S exhibits a main pore size distribution of 8.0 nm, while the main pore size distribution of PtPdCu-HS is reduced to 2.8 nm after nitric acid treatment, which can be ascribed to the formation of surface mesopores of PtPdCu-HS after etching. The surface chemical states of PtPdCu-S and PtPdCu-HS were further analysed by X-ray photoelectron spectroscopy (XPS). It can be seen from Figure 2c that Pt has diverse valence states such as Pt(0) (metallic Pt) and Pt(II) (PtO and $Pt(OH)_2$) in these catalysts. Owing to the higher electronegativity of Pt (2.28) than that of Pd (2.20) and Cu (1.90), usually Pt atoms will withdraw electron density from Pd and Cu in their alloys, giving an increased electron density on Pt.[44,45] Thus, after removal of most Pd and Cu from PtPdCu-S, the Pt(0) $4f_{5/2}$ peak of PtPdCu-HS shifts 0.4 eV to a higher binding energy in contrast to that of PtPdCu-S. Such an interaction between Pt and alloying atoms in PtPdCu-HS could contribute to the enhanced electron

transfer, enhanced ability of CO removal, improved MOR activity and stability compared to PtPdCu-S.[46] The Pd 3d and Cu 2p signals of PtPdCu-S and PtPdCu-HS are shown in Figure 2d and e. After HNO_3 treatment, the surface concentrations of Pd and Cu of PtPdCu-HS are too low to be detected by XPS and the signals are not as obvious as that of PtPdCu-S, indicating a Pt-rich surface of PtPdCu-HS, which is in agreement with the EDX elemental mapping results (Figure 1i-m).

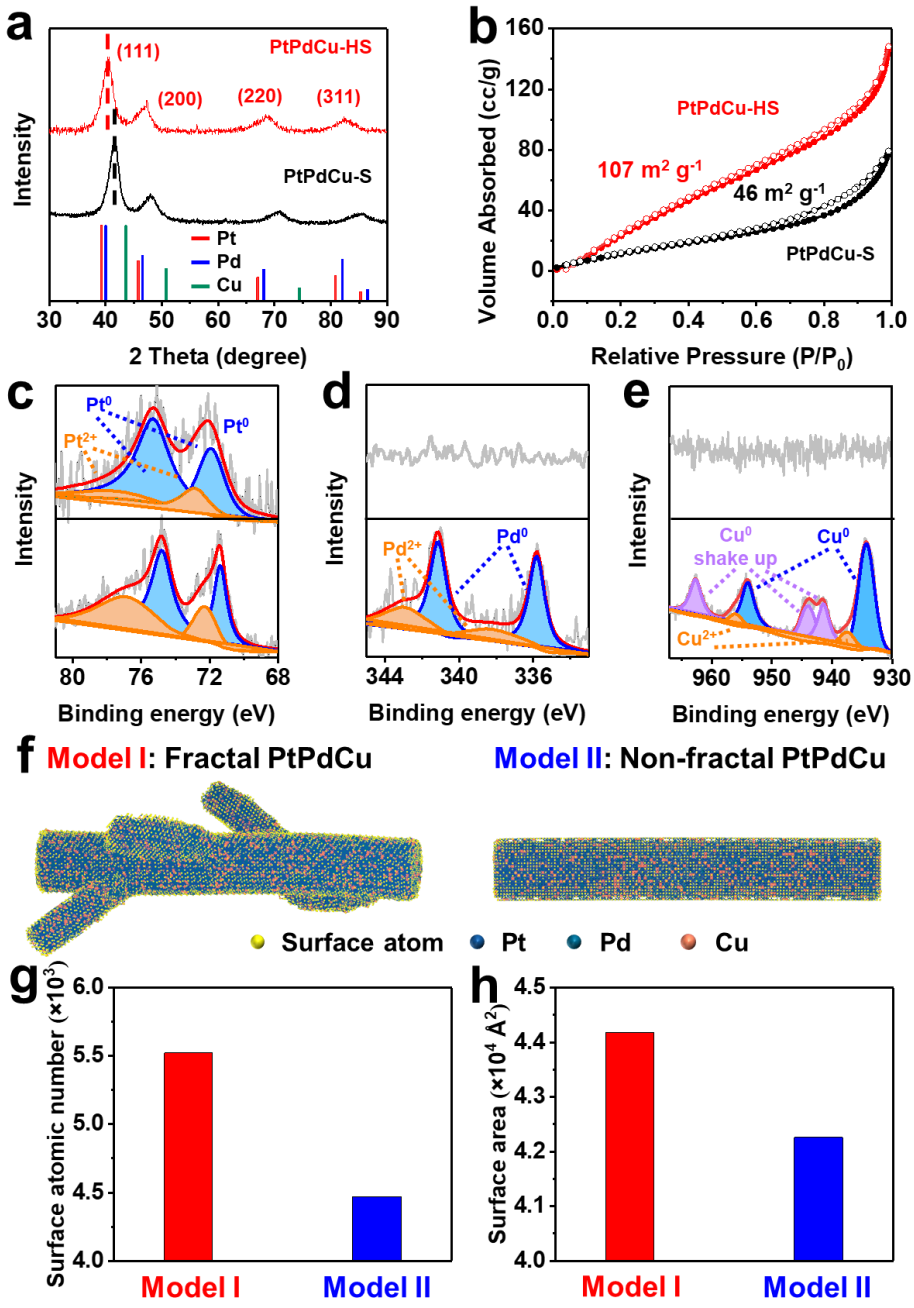

Figure 2. (a) XRD patterns, (b) nitrogen adsorption/desorption isotherms, and XPS spectra showing the (c) Pt 4f, (d) Pd 3d and (e) Cu 2p signals of PtPdCu-HS (up) and PtPdCu-S (down). (f) Calculated models showing the surface atom distribution of fractal and non-fractal PtPdCu. Calculated results showing the comparison of (g) surface atomic number and (h) surface area for Model I and Model II.

In order to gain insight into the formation process of hierarchical fractal PtPdCu sponges, a time-dependent experiment was carried out and the reaction process was monitored through scanning electron microscopy (SEM). As can be seen from Figure S6, the fractal structure was fast formed in 5 minutes, and prolonged reaction time only control the atomic ratio and pore structure. Moreover, the compositional control experiments in Figure S7 proved Cu plays the key role in forming the fractal sponges, and the synergetic reduction of Pd and Pt precursors can be considered to lead to the formation of the surface porous structure for fractal PtPdCu sponges.

To further examine the advances of the fractal structures, DFT calculations were made to characterize the surface atoms and surface area. Two models representing fractal and non-fractal structures were built with a Pt, Pd, Cu atomic ratio of 8:1:1, as shown in Figure 2f. The blue, cyan, orange, and yellow atoms represent Pt, Pd, Cu, and surface atoms, respectively. Compared to non-fractal PtPdCu, fractal PtPdCu exhibited 23.5% higher surface atomic number (Figure 2g) as well as 4.3% higher surface area (Figure 2h), which should lead to more exposed active sites, higher mass transfer accessibility, and thus better catalytic performance.

Due to their unique fractal tri-metallic hollow structure with high surface porosity, PtPdCu-HS are expected to show superior performance in electrocatalysis. The catalytic activity of PtPdCu-HS toward MOR was studied using a three-electrode system. As reference materials, homemade PtPdCu networks (denoted as PtPdCu-N; see Figure S8 for their structural characterization), PtCu hollow sponges (denoted as PtCu-HS; see Figure S9 for their structural characterization) together with commercial Pt/C were also tested for comparison. Figure 3a illustrates cyclic voltammetry (CV) curves of different samples in N_2-saturated 0.1 M $HClO_4$ solution between 0.05 and 1.2 V at a sweep rate of 50 mV s^{-1}. The specific electrochemical active surface area (ECSA) of PtPdCu-HS, PtPdCu-N, PtCu-HS and commercial Pt/C catalysts were

calculated by measuring the charges collected in the hydrogen adsorption/desorption region (0.05-0.35 V) after double-layer correction and assuming a hydrogen monolayer adsorption electron of 210 μC cm^2.[47,48] As shown in Figure 3b, the ECSA of the PtPdCu-HS (41.3 m^2 g^{-1}) was found to be higher than that of PtPdCu-N (33.3 m^2 g^{-1}) and PtCu-HS (37.1 m^2 g^{-1}), which can be ascribed to more exposure of the interior and exterior surface and remarkably high surface area. However, compared to the commercial Pt/C (78.8 m^2 g^{-1}), the ECSA of PtPdCu-HS is smaller due to its large overall structure. Figure 3c shows the CV curves of PtPdCu-HS, PtPdCu-N, PtCu-HS and commercial Pt/C in N_2-purged 0.1 M $HClO_4$ and 1 M CH_3OH solution at a scan rate of 50 mV s^{-1}. PtPdCu-HS gives a mass activity of 1.34 mA μg_{Pt}^{-1}, which is about 2.4, 2.2 and 3.9 times that of PtPdCu-N (0.555 mA μg_{Pt}^{-1}), PtCu-HS (0.603 mA μg_{Pt}^{-1}) and commercial Pt/C catalyst (0.343 mA μg_{Pt}^{-1}), respectively (Figure 3d). Moreover, the specific activity of PtPdCu-HS (3.24 mA cm^{-2}) is about 1.9, 2.0 and 7.3 times that of PtPdCu-N (1.67 mA cm^{-2}), PtCu-HS (1.62 mA cm^{-2}) and commercial Pt/C (0.441 mA cm^{-2}), respectively (Figure 3e). The electrocatalytic performances of PtPdCu-HS, PtPdCu-N, PtCu-HS, and commercial Pt/C are summarized in Table S2. Notably, the catalytic performance of PtPdCu-HS is also superior to that of other previously reported Pt-based catalysts (Table S3). Considering that Pt-based catalysts can be easily poisoned by CO-like intermediate species during MOR, impeding further reactions, we evaluated the CO tolerance of PtPdCu-HS by CO-stripping. Figure 3f compares CO-stripping curves of PtPdCu-HS, PtPdCu-N, PtCu-HS and commercial Pt/C in 1.0 M $HClO_4$ solution. The onset overpotential of the CO electro-oxidation on PtPdCu-HS is 0.767 V, which is much lower than that of PtPdCu-N (0.841 V), PtCu-HS (0.846 V) and commercial Pt/C (0.851 V), implying a significant increase of CO resistance ability.[49,50] The improved anti-poisoning ability of PtPdCu-HS likely originates from the abundant hollow fractal structure with high surface area, allowing the increased formation of adsorbed

oxygen containing species (such as OH^-).[51] These oxygen containing species will exert electronic effect on poisonous CO_{abs} species that are absorbed on adjacent Pt surfaces and will aid the removal of these adsorbed poisonous species CO_{abs} as CO_2.[52] On the other hand, the ease of CO removal from PtPdCu-HS may reflect the effectiveness of electron coupling between the Pt, Pd and Cu in the alloyed nanoparticles.[53] Moreover, the superior CO tolerance of PtPdCu-HS catalyst can be also explained by the surface of PtPdCu nanoparticles being enclosed with the (111) planes, as the adsorption of poisoning species is lowest on Pt (111).[54]

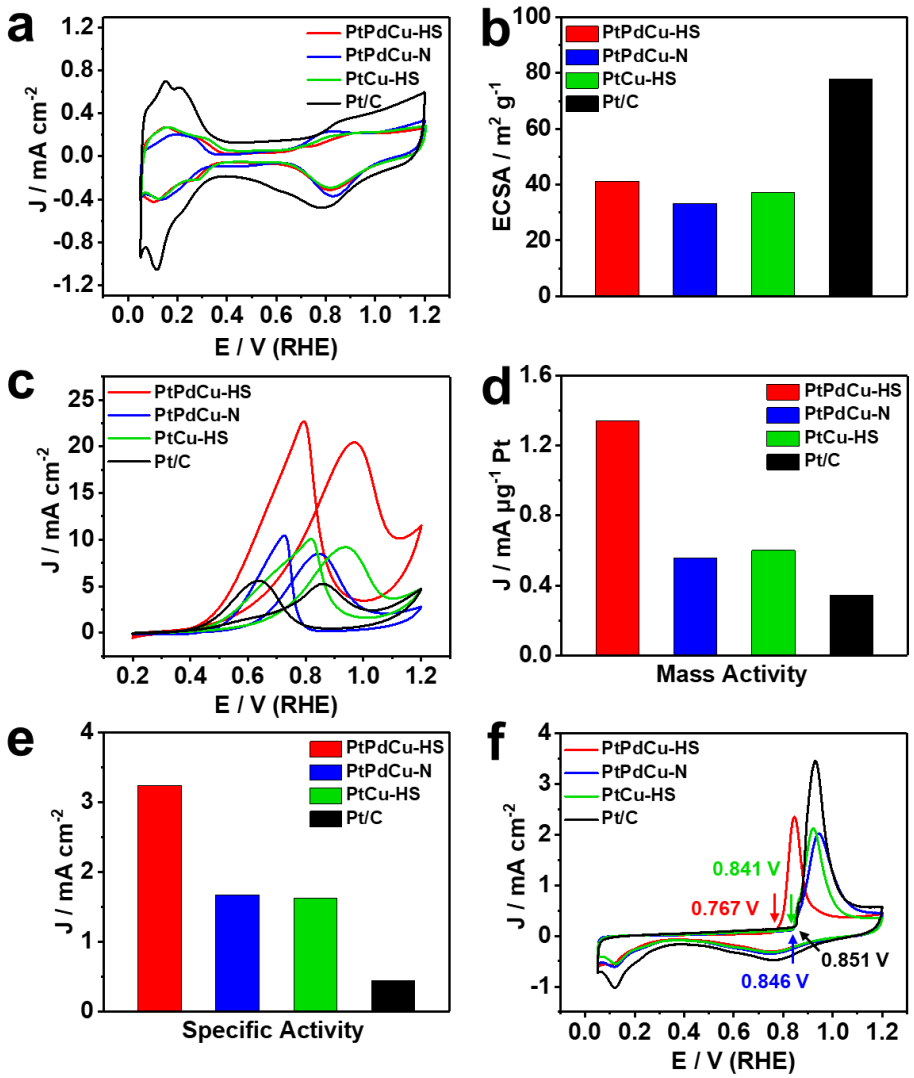

Figure 3. (a) CV curves, (b) ECSA, (C) CVs for methanol oxidation, (d) mass activity, (e) specific activity and (f) CO stripping of PtPdCu-HS, PtPdCu-N, PtCu-HS and commercial Pt/C.

The accelerated durability tests (ADTs) were conducted by performing 2000 potential cycles between 0.2 and 1.2 V versus reversible hydrogen electrode (RHE) in 0.1 M $HClO_4$ and 1.0 M CH_3OH solution with a sweep rate of 50 mV s^{-1} at room temperature. The changes in CV curves of PtPdCu-HS, PtPdCu-N, PtCu-HS and commercial Pt/C before and after ADTs are shown in Figure 4. With increasing numbers of CV cycles, PtPdCu-HS displays a slight drop for the values of current densities (Figure 4a). In contrast, the values of current densities for PtPdCu-N, PtCu-HS and commercial Pt/C exhibit conspicuous drops (Figure 4b-d). The result demonstrates that the electrochemical durability of PtPdCu-HS is also much superior to that of PtPdCu-N, PtCu-HS and commercial Pt/C. Figure 4e shows the calculated mass activity of the four catalysts after ADTs. After 2000 cycles, PtPdCu-HS exhibits mass activity of 1.08 mA μg_{Pt}^{-1}, which is about 2.5, 2.9 and 5.1 times that of PtPdCu-N (0.426 mA μg_{Pt}^{-1}), PtCu-HS (0.375 mA μg_{Pt}^{-1}) and commercial Pt/C catalyst (0.213 mA μg_{Pt}^{-1}), respectively. Meanwhile, the remained mass activity for PtPdCu-HS is 80.6%, much better than PtPdCu-N (71.0%), PtCu-HS (67.6%) and commercial Pt/C (62.1%). Besides, TEM characterizations further prove the high structural stability of PtPdCu-HS after ADTs (Figure S10). Therefore, wherever compared to nonfratcal catalyst (PtPdCu networks), bimetallic catalyst (fratcal PtCu hollow sponges) and commerical catalyst (commercial Pt/C), the fractal trimetallic PtPdCu hollow sponges have demonstrated a greatly improved MOR activity and durability. Moreover, as can be seen in Figure S10, the fractal structure of PtPdCu-HS after ADTs remained unchanged and the nanoparticles still kept high dispersion without aggregation, which explains the high stability of PtPdCu-HS.

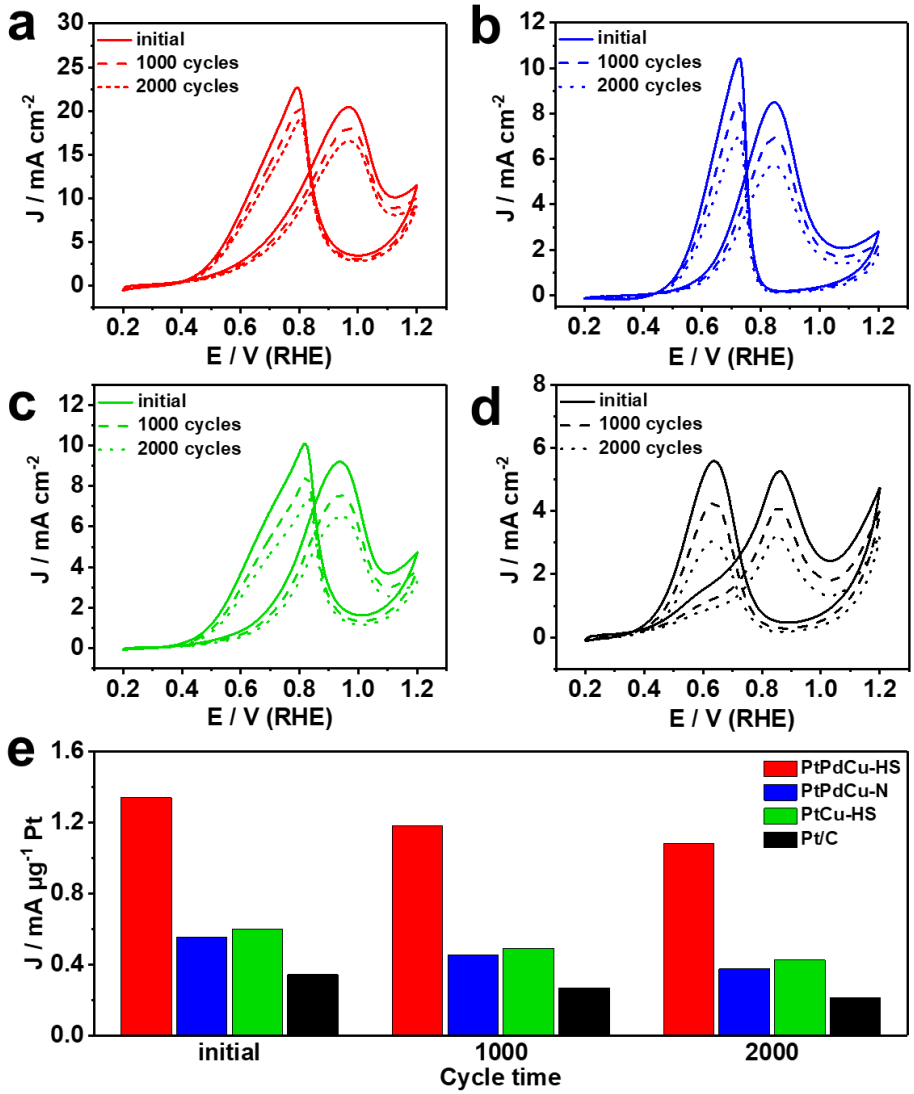

Figure 4. CVs for methanol oxidation of (a) PtPdCu-HS, (b) PtPdCu-N, (c) PtCu-HS and (d) commercial Pt/C after different cycles. (e) Mass activity of PtPdCu-HS, PtPdCu-N, PtCu-HS and (d) commercial Pt/C after different cycles.

The synthesis scheme of PtPdCu-HS is depicted in Figure 5a. When the metal precursors react with Al foil, Pt, Pd and Cu began to be reduced and PtPdCu clusters were quickly formed (i and ii in Figure 5a). With the extension of time, the clusters evolved into fractal structures, and

gradually grew to PtPdCu sponges with a Cu-rich alloy structure (iii in Figure 5a). To further synthesize PtPdCu-HS, PtPdCu-S was treated by HNO_3 to remove most of the Pd and Cu, resulting in a Pt-rich structure (iv in Figure 5a). Notably, PtPdCu-HS synthesized through this method not only has a fractal structure, but also possesses fractal pores. A directed transfer effect mechanism is proposed for the superior electrocatalytic performance of PtPdCu-HS. On the one hand, owing to the thicker pore wall of the main pore compared to the sub-pore ($d_1 > d_2$, as proved by TEM image in Figure 1h), the electrical resistance of the wall of the main pore is smaller than that of the sub-pore ($R_1 < R_2$) according to the resistivity formula[55] (Formula I; derived from $\rho = RS/L$ and $S = \pi(d/2)^2$, where ρ, R, S, L, and d are the resistivity, resistance, section area, length, and diameter of the wall, respectively), resulting in the directed electron transfer from the thicker wall of main pore to the thinner wall of sub-pore, which will make the metal atoms highly active for the capture of methanol molecules. On the other hand, the size of the sub-pore is smaller than the main pore ($D_1 < D_2$), the mass-transfer rate in the sub-pore will be faster than the main pore ($V_1 > V_2$) according to the fluid formula[56] (Formula II; derived from $V = Q/A$ and $A = \pi(D/2)^2$, where V and Q are the transfer velocity and flow rate of the transported mass, A and D are the section area and diameter of the pore, respectively). This could result in the directed mass transfer from the sub-pore to the main pore, facilitating the maximum exploitation of inner active Pt sites.

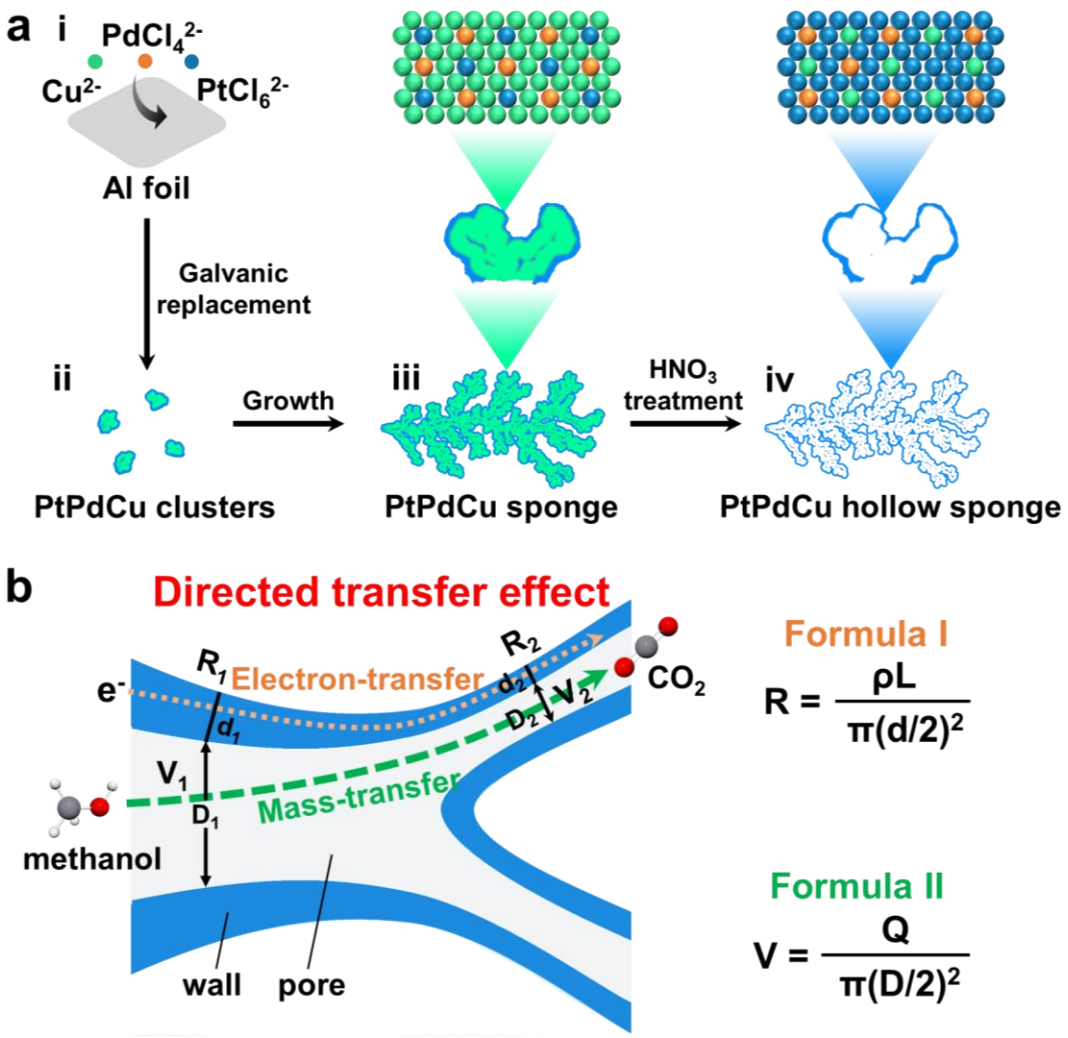

Figure 5. (a) Scheme illustration of the synthesis of PtPdCu hollow sponges: (i) Galvanic replacement between metal precursors and Al foil; (ii) PtPdCu clusters; (iii) Fractal PtPdCu sponges with Cu-rich alloy structure; (iv) Fractal PtPdCu hollow sponges with Pt-rich alloy structure. (b) Scheme illustration of the directed mass- and electron-transfer effect mechanism in PtPdCu-HS.

In summary, we have presented a simple galvanic replacement method for the synthesis of efficient and durable hierarchical fractal PtPdCu sponges toward the MOR. The growth mechanism involved in the morphological evolution and the role of composition have been

illustrated. DFT results demonstrate that the fractal structure exhibits 23.5% higher surface atomic number as well as 4.3% higher surface area in comparison with non-fractal structures. The unique structure of PtPdCu-HS, including overall fractal morphology, hollow nanostructure, mesoporous surface as well as trimetallic alloy, facilitates CO removal and endows the catalyst with high activity and stability. Wherever compared to nonfractal catalysts, bimetallic catalysts or commercial catalysts, the ternary hierarchically fractal PtPdCu sponges with high surface porosity have exhibited notable improved catalytic activity, superior CO tolerance and enhanced electrochemical durability for the MOR. The mechanism for the superior MOR activity of PtPdCu-HS can be reasonably attributed to the directed mass- and electron-transfer brought about by the hierarchical fractal pore structure, which facilitates reactant capture and the maximum exploitation of inner active Pt sites.

ASSOCIATED CONTENT

Supporting Information.

The Supporting Information is available free of charge at http://pubs.acs.org.

Experimental details, particle size distribution, TEM and SEM images, XRD patterns, electrochemical test results.

AUTHOR INFORMATION

Corresponding Author

*Email: yingj5@mail.sysu.edu.cn (J.Y.); xyyang@whut.edu.cn, xyyang@seas.harvard.edu (X.Y.Y.)

Author Contributions

Y.X.X. and X.Y. did the experiments of synthesis and electrocatalytic performance. J.Y. and X.Y.Y. conceived the project, provided the idea, and designed the experiments. G.T. performed the TEM and EDS characterizations. Y.X.Z. and J.B.C. performed the DFT calculation and analysis. Y.W. provided guidance for the synthesis and electrocatalysis. Y.X.X., J.Y. and X.Y.Y. wrote and revised the paper. M.D.S. and K.I.O. revised the paper. J.W. provided help with the TEM and EDS characterizations. All the authors discussed results and analyzed the data, and have given approval to the final version of the manuscript.

Notes

The authors declare no competing financial interest.

ACKNOWLEDGMENT

This work was supported by a joint National Natural Science Foundation of China-Deutsche Forschungsgemein-schaft (NSFC-DFG) project (NSFC grant 51861135313, DFG JA466/39-1), Sino-German Center COVID-19 Related Bilateral Collaborative project (C-0046), Jilin Province Science and Technology Development Plan (20180101208JC), FRFCU (19lgzd16, 20lgpy77), ISTCP (2015DFE52870), Guangdong Basic and Applied Basic Research Foundation (No. 2019A1515110436), and Guangdong Province International Scientific and Technological Cooperation Projects (2020A0505100036). The S/TEM work was performed at the Nanostructure Research Centre (NRC), which is supported by the Fundamental Research Funds for the Central Universities (WUT: 2019III012GX).

REFERENCES

(1) Wang, Y.-J.; Zhao, N.; Fang, B.; Li, H.; Bi, X. T.; Wang, H. Carbon-Supported Pt-Based Alloy Electrocatalysts for the Oxygen Reduction Reaction in Polymer Electrolyte Membrane Fuel Cells: Particle Size, Shape, and Composition Manipulation and Their Impact to Activity. *Chem. Rev.* **2015**, 115, 3433-3467.

(2) Huang, X.; Zhao, Z.; Cao, L.; Chen, Y.; Zhu, E.; Lin, Z.; Li, M.; Yan, A.; Zettl, A.; Wang, Y. M.; Duan, X.; Mueller, T.; Huang, Y. High-performance transition metal-doped Pt3Ni octahedra for oxygen reduction reaction. *Science* **2015**, 348, 1230-1234.

(3) Li, J.; Yin, H.-M.; Li, X.-B.; Okunishi, E.; Shen, Y.-L.; He, J.; Tang, Z.-K.; Wang, W.-X.; Yücelen, E.; Li, C.; Gong, Y.; Gu, L.; Miao, S.; Liu, L.-M.; Luo, J.; Ding, Y. Surface evolution of a Pt-Pd-Au electrocatalyst for stable oxygen reduction. *Nat. Energy* **2017**, 2, 17111.

(4) Li, H.-H.; Fu, Q.-Q.; Xu, L.; Ma, S.-Y.; Zheng, Y.-R.; Liu, X.-J.; Yu, S.-H. Highly crystalline PtCu nanotubes with three dimensional molecular accessible and restructured surface for efficient catalysis. *Energy Environ. Sci.* **2017**, 10, 1751-1756.

(5) Wang, H.; Xu, S.; Tsai, C.; Li, Y.; Liu, C.; Zhao, J.; Liu, Y.; Yuan, H.; Abild-Pedersen, F.; Prinz, F. B.; Nørskov, J. K.; Cui, Y. Direct and continuous strain control of catalysts with tunable battery electrode materials. *Science* **2016**, 354, 1031-1036.

(6) Li, M.; Zhao, Z.; Cheng, T.; Fortunelli, A.; Chen, C.-Y.; Yu, R.; Zhang, Q.; Gu, L.; Merinov, B.; Lin, Z.; Zhu, E.; Yu, T.; Jia, Q.; Guo, J.; Zhang, L.; Goddard III, W. A.; Huang, Y.; Duan, X. Ultrafine jagged platinum nanowires enable ultrahigh mass activity for the oxygen reduction reaction. *Science* **2016**, 354, 1414-1419.

(7) Bu, L.; Zhang, N.; Guo, S.; Zhang, X.; Li, J.; Yao, J.; Wu, T.; Lu, G.; Ma, J.-Y.; Su, D.; Huang, X. Biaxially strained PtPb/Pt core/shell nanoplate boosts oxygen reduction catalysis. *Science* **2016**, 354, 1410-1414.

(8) Xie, Y.; Cai, J.; Wu, Y.; Zang, Y.; Zheng, X.; Ye, J.; Cui, P.; Niu, S.; Liu, Y.; Zhu, J.; Liu, X.; Wang, G.; Qian, Y. Boosting Water Dissociation Kinetics on Pt-Ni Nanowires by N-Induced Orbital Tuning. *Adv. Mater.* **2019**, 31, 1807780.

(9) Xiao, Y.-X.; Ying, J.; Tian, G.; Tao, Y.; Wei, H.; Fan, S.-Y.; Sun, Z.-H.; Zou, W.-J.; Hu, J.; Chang, G.-G.; Li, W.; Yang, X.-Y.; Janiak, C. Highly dispersed PtPd on graphitic nanofibers and its heavy d-π effect. *Applied. Catal. B-Environ.* **2019**, 259, 118080.

(10) Zhang, L.; Roling, L. T.; Wang, X.; Vara, M.; Chi, M.; Liu, J.; Choi, S.-I.; Park, J.; Herron, J. A.; Xie, Z.; Mavrikakis, M.; Xia, Y. Platinum-based nanocages with subnanometer-thick walls and well-defined, controllable facets. *Science* **2015**, 349, 412-416.

(11) Niu, Z.; Becknell, N.; Yu, Y.; Kim, D.; Chen, C.; Kornienko, N.; Somorjai, G. A.; Yang, P. Anisotropic phase segregation and migration of Pt in nanocrystals en route to nanoframe catalysts. *Nat. Mater.* **2016**, 15, 1188-1194.

(12) Jiang, B.; Li, C.; Tang, J.; Takei, T.; Kim, J. H.; Ide, Y.; Henzie, J.; Tominaka, S.; Yamauchi, Y. Tunable-Sized Polymeric Micelles and Their Assembly for the Preparation of Large Mesoporous Platinum Nanoparticles. *Angew. Chem. Int. Ed.* **2016**, 55, 10037-10041.

(13) Ying, J.; Jiang, G.; Cano, Z. P.; Ma, Z.; Chen, Z. Spontaneous weaving: 3D porous PtCu networks with ultrathin jagged nanowires for highly efficient oxygen reduction reaction. *Appl. Catal. B* **2018**, 236, 359-367.

(14) Xiao, Y.-X.; Ying, J.; Tian, G.; Zhang, X.-Q.; Janiak, C.; Ozoemena, K. I.; Yang, X.-Y. PtPd hollow nanocubes with enhanced alloy effect and active facets for efficient methanol oxidation reaction. *Chem. Commun.* **2021**, 57, 986-989.

(15) Yang, P.; Wu, Z.; Jiang, Y.; Pan, Z.; Tian, W.; Jiang, L.; Hu, L. Fractal $(Ni_xCo_{1-x})_9Se_8$ Nanodendrite Arrays with Highly Exposed (011) Surface for Wearable, All-Solid-State Supercapacitor. *Adv. Energy Mater.* **2018**, 8, 1801392.

(16) James, S.; Contractor, R. Study on Nature-inspired Fractal Design-based Flexible Counter Electrodes for Dye-Sensitized Solar Cells Fabricated using Additive Manufacturing. *Sci. Rep.* **2018**, 8, 17032.

(17) Hou, C.; Meng, G.; Huang, Q.; Zhu, C.; Huang, Z.; Chen, B.; Sun, K. Ag-nanoparticle-decorated Au-fractal patterns on bowl-like-dimple arrays on Al foil as an effective SERS substrate for the rapid detection of PCBs. *Chem. Commun.* **2014**, 50, 569-571.

(18) Chen, L.-H.; Sun, M.-H.; Wang, Z.; Yang, W.; Xie, Z.; Su, B.-L. Hierarchically Structured Zeolites: From Design to Application. *Chem. Rev.* **2020**, 120, 20, 11194-11294.

(19) Chen, X.; Cui, C.-H.; Guo, Z.; Liu, J.-H.; Huang, X.-J.; Yu, S.-H. Unique Heterogeneous Silver-Copper Dendrites with a Trace Amount of Uniformly Distributed Elemental Cu and Their Enhanced SERS Properties. *Small* **2011**, 7, 858-863.

(20) Li, D.; Liu, J.; Wang, H.; Barrow, C. J.; Yang, W. Electrochemical synthesis of fractal bimetallic Cu/Ag nanodendrites for efficient surface enhanced Raman spectroscopy. *Chem. Commun.* **2016**, 52, 10968-10971.

(21) Wang, L.; Zhu, S.; Shen, M.; Tian, H.; Xie, S.; Zhang, H.; Zhang Y.; Tang, Y. Fractal MTW Zeolite Crystals: Hidden Dimensions in Nanoporous Materials. *Angew. Chem. Int. Ed.* **2017**, 56, 11764-11768.

(22) Zhao, Y.; Ye, Z.; Wang, L.; Zhang, H.; Xue, F.; Xie, S.; Cao, X.-M.; Zhang, Y.; Tang, Y. Engineering Fractal MTW Zeolite Mesocrystal: Particle-Based Dendritic Growth via Twinning-Plane Induced Crystallization. *Cryst. Growth Des.* **2018**, 18, 1101-1108.

(23) Geng, D.; Wu, B.; Guo, Y.; Luo, B.; Xue, Y.; Chen, J.; Yu, G.; Liu, Y. Fractal Etching of Graphene. *J. Am. Chem. Soc.* **2013**, 135, 6431-6434.

(24) Fang, J.; Wang, D.; DeVault, C. T.; Chung, T.-F.; Chen, Y. P.; Boltasseva, A.; Shalaev, V. M.; Kildishev, A. V. Enhanced Graphene Photodetector with Fractal Metasurface. *Nano Lett.* **2017**, 17, 57-62.

(25) Massicotte, M.; Yu, V.; Whiteway, E.; Vatnik, D.; Hilke, M. Quantum Hall effect in fractal graphene: growth and properties of graphlocons. *Nanotechnology* **2013**, 24, 325601.

(26) Sharma, V.; Ali-Löytty, H.; Koivikko, A.; Yiannacou, K.; Lahtonen, K.; Sariola, V. Copper Oxide Microtufts on Natural Fractals for Efficient Water Harvesting. *Langmuir* **2021**, 37, 3370-3381.

(27) Sun, Z.; Firdoz, S.; Yap, E. Y.-X.; Li, L.; Lu, X. Hierarchically structured MnO_2 nanowires supported on hollow Ni dendrites for high-performance supercapacitors. *Nanoscale* **2013**, 5, 4379-4387.

(28) Li, D.; Zheng, Z.; Lei, Y.; Ge, S.; Zhang, Y.; Zhang, Y.; Wong, K. W.; Yang, F.; Lau, W. M. Design and growth of dendritic $Cu_{2-x}Se$ and bunchy CuSe hierarchical crystalline aggregations. *CrystEngComm* **2010**, 12, 1856-1861.

(29) Zhang, P.; Chen, L.; Xu, T.; Liu, H.; Liu, X.; Meng, J.; Yang, G.; Jiang, L.; Wang, S. Programmable Fractal Nanostructured Interfaces for Specific Recognition and Electrochemical Release of Cancer Cells. *Adv. Mater.* **2013**, 25, 3566-3570.

(30) Yang, C.; Cui, X.; Zhang, Z.; Chiang, S. W.; Lin, W.; Duan, H.; Li, J.; Kang, F.; Wong, C.-P. Fractal dendrite-based electrically conductive composites for laser-scribed flexible circuits. *Nat. Commun.* **2015**, 6, 8150.

(31) Zhu, Q.; Yang, D.; Liu, H.; Sun, X.; Chen, C.; Bi, J.; Liu, J.; Wu, H.; Han, B. Hollow Metal-Organic-Framework-Mediated In Situ Architecture of Copper Dendrites for Enhanced CO_2 Electroreduction. *Angew. Chem. Int. Ed.* **2020**, 59, 8896-8901.

(32) Cui, X.; Xiao, P.; Wang, J.; Zhou, M.; Guo, W.; Yang, Y.; He, Y.; Wang, Z.; Yang, Y.; Zhang, Y.; Lin, Z. Highly Branched Metal Alloy Networks with Superior Activities for the Methanol Oxidation Reaction. *Angew. Chem. Int. Ed.* **2017**, 56, 4488-4493.

(33) Chang, R.; Zheng, L.; Wang, C.; Yang, D.; Zhang, G.; Sun, S. Synthesis of hierarchical platinum-palladium-copper nanodendrites for efficient methanol oxidation. *Appl. Catal. B* **2017**, 211, 205-211.

(34) Zhang, G.; Sun, S.; Cai, M.; Zhang, Y.; Li, R.; Sun, X. Porous Dendritic Platinum Nanotubes with Extremely High Activity and Stability for Oxygen Reduction Reaction. *Sci. Rep.* **2013**, 3, 1526.

(35) El-Nagar, G. A.; Muench, F.; Roth, C. Tailored dendritic platinum nanostructures as a robust and efficient direct formic acid fuel cell anode. *New J. Chem.* **2019**, 43, 4100-4105.

(36) Chen, S.; Su, H.; Wang, Y.; Wu, W.; Zeng, J. Size-Controlled Synthesis of Platinum-Copper Hierarchical Trigonal Bipyramid Nanoframes. *Angew. Chem. Int. Ed.* **2015**, 54, 108-113.

(37) Lin, L.; Sun, Z.; Yuan, M.; He, J.; Long, R.; Li, H.; Nan, C.; Sun, G.; Ma, S. Significant enhancement of the performance of hydrogen evolution reaction through shape-controlled synthesis of hierarchical dendrite-like platinum. *J. Mater. Chem. A* **2018**, 6, 8068-8077.

(38) Nosheen, F.; Zhang, Z.; Xiang, G.; Xu, B.; Yang, Y.; Saleem, F.; Xu, X.; Zhang, J.; Wang, X. Three-dimensional hierarchical Pt-Cu superstructures. *Nano Res.* **2015**, 8, 832-838.

(39) Zhang, H.; Wang, H.; Cao, J.; Ni, Y. Hierarchical Cu-Ni-Pt dendrites: Two-step electrodeposition and highly catalytic performances. *J. Alloys Compd.* **2017**, 698, 654-661.

(40) Liu, J.; Wang, X.; Lin, Z.; Cao, Y.; Zheng, Z.Z.; Zeng, Z.; Hu, Z. Shape-Controllable Pulse Electrodeposition of Ultrafine Platinum Nanodendrites for Methanol Catalytic Combustion and the Investigation of their Local Electric Field Intensification by Electrostatic Force Microscope and Finite Element Method. *Electrochim. Acta* **2014**, 136, 66-74.

(41) Liu, J.; Cao, L.; Huang, W.; Li, Z. Direct electrodeposition of PtPd alloy foams comprised of nanodendrites with high electrocatalytic activity for the oxidation of methanol and ethanol. *J. Electroanal. Chem.* **2012**, 686, 38-45.

(42) Ying, J.; Jiang, G.; Cano, Z. P.; Han, L.; Yang, X.-Y.; Chen, Z. Nitrogen-doped hollow porous carbon polyhedrons embedded with highly dispersed Pt nanoparticles as a highly efficient and stable hydrogen evolution electrocatalyst. *Nano Energy* **2017**, 40, 88-94.

(43) Shen, L.; Ying, J.; Tian, G.; Jia, M.; Yang, X.-Y. Ultralong PtPd Alloyed Nanowires Anchored on Graphene for Efficient Methanol Oxidation Reaction. *Chem Asian J.* **2021**, 16, 1130-1137.

(44) Wang, K.; Du, H.; Sriphathoorat, R.; Shen, P. K. Vertex-Type Engineering of Pt-Cu-Rh Heterogeneous Nanocages for Highly Efficient Ethanol Electrooxidation. *Adv. Mater.* **2018**, 30, 1804074.

(45) Lee, Y.-W.; Lee, J.-Y.; Kwak, D.-H.; Hwang, E.-T.; Sohn, J. I.; Park, K.-W. Pd@Pt core-shell nanostructures for improved electrocatalytic activity in methanol oxidation reaction. *Appl. Catal. B* **2015**, 179, 178-184.

(46) Wang, Y.; Yu, H.-Z.; Ying, J.; Tian, G.; Liu, Y.; Geng, W.; Hu, J.; Lu, Y.; Chang, G.-G.; Ozoemena, K. I.; Janiak, C.; Yang, X.-Y. Ultimate Corrosion to Pt-Cu Electrocatalysts for Enhancing Methanol Oxidation Activity and Stability in Acidic Media. *Chem. Eur. J.* **2021**, 10.1002/chem.202100754.

(47) Lim, B.; Jiang, M.; Camargo, P. H. C.; Cho, E. C.; Tao, J.; Lu, X.; Zhu, Y.; Xia, Y. Pd-Pt bimetallic nanodendrites with high activity for oxygen reduction. *Science* **2009**, 324, 1302-1305.

(48) Ying, J.; Li, J.; Jiang, G.; Cano, Z. P.; Ma, Z.; Zhong, C.; Su, D.; Chen, Z. Metal-organic frameworks derived platinum-cobalt bimetallic nanoparticles in nitrogen-doped hollow porous carbon capsules as a highly active and durable catalyst for oxygen reduction reaction. *Appl. Catal. B* **2018**, 225, 496-503.

(49) Zhao, Y.; Liu, J.; Liu, C.; Wang, F.; Song, Y. Amorphous CuPt Alloy Nanotubes Induced by $Na_2S_2O_3$ as Efficient Catalysts for the Methanol Oxidation Reaction. *ACS Catal.* **2016**, 6, 4127-4134.

(50) Tang, B.; Lv, Y.; Du, J.; Dai, Y.; Pan, S.; Xie, Y.; Zou, J. MoS_2-Coated Ni_3S_2 Nanorods with Exposed {110} High-Index Facets As Excellent CO-Tolerant Cocatalysts for Pt: Ultradurable Catalytic Activity for Methanol Oxidation. *ACS Sustainable Chem. Eng.* **2019**, 7, 11101-11109.

(51) Zeng, J.; Yang, J.; Lee, J. Y.; Zhou, W. Preparation of Carbon-Supported Core-Shell Au-Pt Nanoparticles for Methanol Oxidation Reaction: The Promotional Effect of the Au Core. *J. Phys. Chem. B* **2006**, 110, 24606-24611.

(52) Wang, A.-L.; Liang, C.-L.; Lu, X.-F.; Tong, Y.-X.; Li, G.-R. Pt-MoO_3-RGO ternary hybrid hollow nanorod arrays as high-performance catalysts for methanol electrooxidation. *J. Mater. Chem. A* **2016**, 4, 1923-1930.

(53) Du, X.; Luo, S.; Du, H.; Tang, M.; Huang, X.; Shen, P. K. Monodisperse and self-assembled Pt-Cu nanoparticles as an efficient electrocatalyst for the methanol oxidation reaction. *J. Mater. Chem. A* **2016**, 4, 1579-1585.

(54) Kang, Y.; Li, M.; Cai, Y.; Cargnello, M.; Diaz, R. E.; Gordon, T. R.; Wieder, N. L.; Adzic, R. R.; Gorte R. J.; Stach, E. A. Heterogeneous Catalysts Need Not Be so "Heterogeneous": Monodisperse Pt Nanocrystals by Combining Shape-Controlled Synthesis and Purification by Colloidal Recrystallization. *J. Am. Chem. Soc.* **2013**, 135, 2741-2747.

(55) Guo, Y.; Sato, W.; Inoue, K.; Zhang, W.; Yu, G.; Nakamura, E. n-Type doping for efficient polymeric electron-transporting layers in perovskite solar cells. *J. Mater. Chem. A* **2016**, 4, 18852-18856.

(56) Reddy, S.; Reddy, Y. R. Verification of reynolds number by density method. *Int. J. Eng. Sci.* **2018**, 4, 113-116.

For Table of Contents Only